Available online at www.sciencedirect.com
ScienceDirect
Journal of Structural Biology 157 (2007) 201–210
Journal of Structural Biology
www.elsevier.com/locate/yjsbi

Ab initio resolution measurement for single particle structures

Duncan Sousa, Nikolaus Grigorieff *

Howard Hughes Medical Institute and Department of Biochemistry, Rosenstiel Basic Medical Sciences Research Center, Brandeis University, 415 South Street, Waltham, MA 02454, USA

Received 24 April 2006; received in revised form 3 August 2006; accepted 4 August 2006
Available online 15 August 2006

Abstract

A computational method is described that allows the measurement of the signal-to-noise ratio and resolution of a three-dimensional structure obtained by single particle electron microscopy and reconstruction. The method does not rely on the availability of the original image data or the calculation of several structures from different parts of the data that are needed for the commonly used Fourier Shell Correlation criterion. Instead, the correlation between neighboring Fourier pixels is calculated and used to distinguish signal from noise. The new method has been conveniently implemented in a computer program called RMEASURE and is available to the microscopy community.

Keywords: Resolution measurement; Electron microscopy; Protein structure; Single particle; RMEASURE

1. Introduction

Three-dimensional (3D) visualization of isolated (single) macromolecules and their assemblies by transmission electron microscopy has become one of the standard techniques in cell biology to gain insight into the function and mechanism of molecular machines in living cells (Nogales and Grigorieff, 2001). This technique, often referred to as single particle electron microscopy (SPEM), can be applied in cases not easily accessible by more traditional techniques, such as nuclear magnetic resonance (NMR) spectroscopy or X-ray crystallography. It does not require crystals, it does not impose an upper molecular mass limit on the structure under investigation, and it can be applied to only a few pmol of material (see, for example, Jurica et al., 2004; Sokolova et al., 2001). However, unlike NMR and X-ray crystallography, the resolution of structures visualized by SPEM is, so far, limited to about 6 Å or lower, too low to allow interpretation of the structures by atomic models. For example, viruses with icosahedral symmetry can currently be resolved to about 7 Å resolution (Bottcher et al., 1997; Laurinmaki et al., 2005; Zhang et al., 2003; Zhou et al., 2001), the chaperone GroEL (D7 symmetry) was solved to about 6 Å resolution (Ludtke et al., 2004) while the asymmetrical ribosome has been resolved to about 8 Å resolution (Halic et al., 2006). Furthermore, a lower limit of the molecular mass exists because a minimum mass is required to generate sufficient scattering contrast for the alignment of images of the individual particles (Henderson, 1995). Assuming perfect images that are only limited by the electron dose (about 10 electrons/Å^2) and that do not suffer from contrast-degrading effects, a molecule or complex of about 40 kDa should generate sufficient contrast to align images sufficiently accurately to obtain 3 Å resolution. In practice, however, image contrast is degraded by electrostatic charging of the specimen, beam-induced movement, sample drift, and an attenuating envelope of the contrast transfer function (CTF) of the microscope. This increases the lower mass limit. For example, if the image contrast is degraded 50%, the lower mass limit would be about 150 kDa.

Despite the increasing popularity of SPEM, the assessment of the resolution of a reconstruction is still

* Corresponding author. Fax: +1 781 736 2419.
E-mail address: niko@brandeis.edu (N. Grigorieff).

1047-8477/$ - see front matter © 2006 Elsevier Inc. All rights reserved.
doi:10.1016/j.jsb.2006.08.003

controversial. The resolution is a common way to assess the quality of the reconstruction, particularly when it is too low to recognize secondary structure. Different resolution criteria exist (Frank et al., 1981; Harauz and van Heel, 1986; Penczek et al., 1994; Unser et al., 1989, 1987) of which the Fourier Shell Correlation (FSC, Harauz and van Heel, 1986) is the most widely used. The resolution of a reconstruction is often quoted as the point at which the FSC curve drops below 0.5 (Bottcher et al., 1997) or 0.143 (Rosenthal and Henderson, 2003). The resolution assessment is further complicated by the fact that the FSC curve itself can be completely unreliable due to the over-fitting of noise during the refinement of the reconstruction (Grigorieff, 2000; Stewart and Grigorieff, 2004). The term over-fitting refers here to the partial alignment of noise to the reference used in the refinement. Over-fitting of noise reduces the overall resolution that can be achieved in a refinement. Depending on the refinement procedure, it can lead to FSC values much higher than would be expected in an unbiased assessment (Stewart and Grigorieff, 2004). The work presented here describes a new method to assess the resolution of a 3D reconstruction that appears to be less affected by over-fitting. Previous resolution criteria, including the FSC, must be calculated at the time of data processing because they need either the raw data or reconstructions from subsets of the data. In contrast, the new method can be used on a final reconstruction without the need for additional data. The new method relies on a novel correlation function referred to as Fourier Neighbor Correlation (FNC).

2. Theory

2.1. Fourier Neighbor Correlation

The new resolution assessment method takes advantage of the correlation between neighboring terms in the Fourier Transform (FT) of a 3D structure. Such correlations are introduced when the density of a structure occupies only part of the 3D array of pixels representing it on a computer (Shaikh et al., 2003). This 3D array usually has the shape of a cube. The correlation between neighboring terms in the FT of the array can be understood in the following way: if the cube was filled with random noise, the terms in the FT would be entirely uncorrelated. We assume here and in the following that the noise can be represented by a Gaussian distribution with mean zero and standard deviation σ. A 3D mask is applied that resets values outside the mask to zero and leaves non-zero pixels only in part of the cube. This operation can be represented in Fourier space as a convolution of the FT of the mask with the FT of the noise. The convolution introduces correlations between the Fourier terms. For a discrete FT we can write

$$F_{\mathbf{p}} = \frac{U}{V}\sum_{\mathbf{h}} F_{\mathbf{h}} G_{\mathbf{hp}}. \quad (1)$$

$F_{\mathbf{p}}$ is the Fourier term at point $\mathbf{p}$, V is the volume of the cube containing the mask, U is the volume enclosed by the mask, and $G_{\mathbf{hp}}$ is the FT of the mask:

$$G_{\mathbf{hp}} = \int_U e^{2\pi i(\mathbf{p}-\mathbf{h})\mathbf{r}} d\mathbf{r}. \quad (2)$$

If the random noise inside the mask is replaced by a macromolecular structure, the correlation between Fourier terms changes (see below) but will not vanish. Eq. (1) still holds, and is well known in X-ray crystallography where it is used to determine phases by solvent-flattening (Arnold and Rossmann, 1986). In the case of X-ray crystallography, V represents the volume of the unit cell, U is the volume of the molecular structure, $F_{\mathbf{p}}$ is the structure factor of reflection $\mathbf{p}$, and $G_{\mathbf{hp}}$ is the FT of the molecular envelope.

Returning to our example with a mask filled with random noise, we will now consider what we can say about the correlation between neighboring Fourier terms that result from the masking. Fig. 1 depicts the FT of an arbitrary volume. The center of the cube is the origin of the FT. Elements lying on the sphere shown within the cube all have the same distance from the origin, and therefore, originate from features of a certain spatial frequency, i.e., they correspond to a certain resolution. A cluster of seven cubes is also shown and represents neighboring Fourier terms within the transform. To evaluate correlations between neighboring Fourier terms, we consider only the nearest neighbors. Thus, in Fig. 1, the red cube in the center of the cluster has six neighbors. We can now evaluate average correlation coefficients between neighboring Fourier terms by picking a number of locations and calculating correlation coefficients between these locations and their neighbors. We refer to this correlation as the Fourier Neighbor Correlation, or FNC. Since,

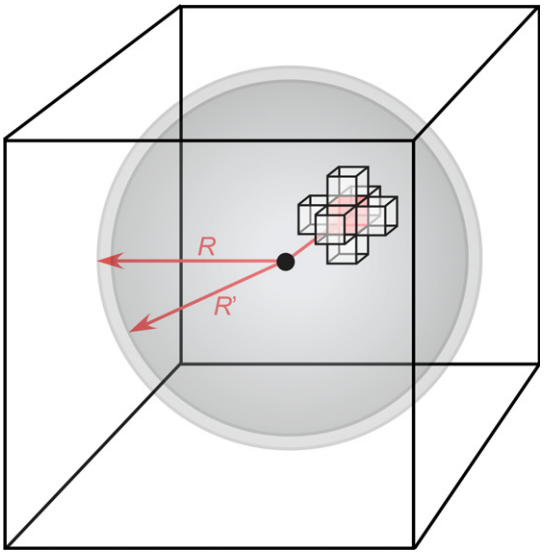

Fig. 1. Fourier Transform of a cubic array of densities. The cluster of small black cubes represents terms in the Fourier Transform neighboring the term represented by the small red cube. Terms in a shell outlined by the two gray spheres with radius R and R', and their neighboring terms, are used to calculate the Fourier Neighbor Correlation (FNC).

later on, we will be interested in evaluating these correlation coefficients as a function of resolution, we pick terms that lie within a thin spherical shell centered on the transform origin. If $p = |\mathbf{p}|$ is the distance of point $\mathbf{p}$ from the origin, a shell at resolution R and thickness $R - R'$ contains all points with $R' < p \leqslant R$. For convenience, we choose the shell thickness to be always one unit within the discrete FT, or $R - R' = 1/L$, where L is the length of one side of the cube containing the mask. The FNC at resolution R is then given by

$$\mathrm{FNC}(R) = \frac{\sum_{\mathbf{p}\in R'<p\leqslant R}\sum_{\mathbf{h}\in N(\mathbf{p})} F_{\mathbf{p}} F^{*}_{\mathbf{h}}}{\sqrt{\sum_{\mathbf{p}\in R'<p\leqslant R}\sum_{\mathbf{h}\in N(\mathbf{p})} |F_{\mathbf{p}}|^2 \sum_{\mathbf{p}\in R'<p\leqslant R}\sum_{\mathbf{h}\in N(\mathbf{p})} |F_{\mathbf{h}}|^2}}. \quad (3)$$

Here, $N(\mathbf{p})$ indicates the six Fourier terms neighboring point $\mathbf{p}$ (see Fig. 1), and $*$ denotes the conjugate complex value.

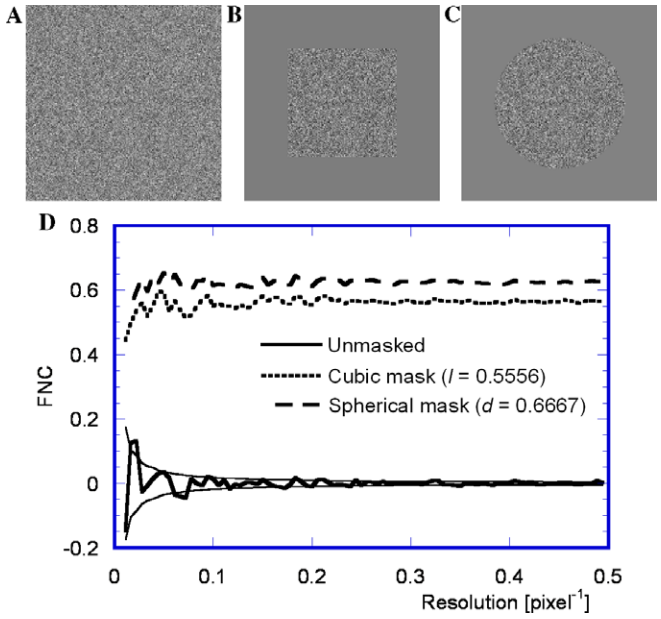

Fig. 2. Plots of the FNC for noise-filled masks of different geometry. (A) Slice through a noise-filled cube representing the unmasked volume of $180 \times 180 \times 180$ pixels. (B) Slice through the cube after applying a cubic mask of $100 \times 100 \times 100$ pixels. (C) Slice through the cube after applying a spherical mask of 120 pixels diameter. (D) FNC plots calculated for the three volumes shown in (A), (B) and (C). The thin lines enveloping the plot for the unmasked volume (thick continuous line) indicate the expected standard deviation of the FNC which is given by $1/\sqrt{N_s}$, where N_s is the number of terms contributing to the correlation coefficient in Eq. (3).

For a cube filled with Gaussian-distributed noise the FNC will, on average, be zero. For a noise-filled mask within the cube, the average correlation is given by the mask transform, $G_{\mathbf{hp}}$, evaluated at neighboring points, i.e., $|\mathbf{p} - \mathbf{h}| = 1$. Since the amplitudes and phases of the Fourier terms of the cube filled with noise are uncorrelated and random, the average FNC will be invariant with resolution R. Fig. 2 shows the FNC calculated for a noise-filled cube, a noise-filled mask within the cube that has the shape of a smaller cube, and a noise-filled spherical mask. As expected, the FNC is approximately constant across the spectrum. The larger variance of the FNC at low resolution reflects the smaller number of terms in the corresponding shells used to calculate the FNC. Table 1 gives the FNC averaged over the entire spectrum in each case. The table also lists the FT of the mask in each case, and the expected average correlation coefficient which is in excellent agreement with the average FNC observed in the plots in Fig. 2.

2.2. Modeling a macromolecular structure

As we shall see later, the FNC calculated for a real macromolecular structure is not constant across the spectrum. To understand the reasons for this deviation, we consider a spherical mask that contains Gaussian-distributed noise with a non-zero average we will refer to as an offset. Fig. 3 shows the FNC for the same spherical mask used in calculations for Fig. 2, but with a range of different offsets for the noise inside the mask. Depending on the magnitude of the offset, compared with σ, the FNC drops to smaller values at low resolution and oscillates over a certain resolution range. In the extreme case of an infinite offset (a solid sphere without noise), the FSC oscillates over the entire spectrum. The periodicity of the oscillations is equal to the periodicity of the mask transform (Table 1). For a solid sphere, the FT periodically changes its sign. At resolution values corresponding to points where the sign changes the FNC will be smaller than at other resolution values, and this leads to the observed oscillation in the FSC. For a solid sphere (and masks of any other shape) filled with noise containing an offset, the average correlation between neighboring Fourier terms is not constant across the spectrum. Compared with the previous case where a mask was applied to a cube filled with noise, a mask filled with a constant value can be thought of as being the result of masking a cube filled with a constant value.

Table 1
Average Fourier Neighbor Correlation (FNC) for different masks filled with Gaussian-distributed noise (see Fig. 2)

Mask	Average FNC	Mask transform $G_{\mathbf{hp}}$	$G_{\mathbf{hp}}$ at $\lvert\mathbf{p} - \mathbf{h}\rvert = 1$
Unmasked	0.0005	$\delta_{\mathbf{ph}}$	0
Cubic mask (side length $l = 0.5556$)	0.5642	$\prod_{i=1}^{3} \frac{\sin[\pi l(p_i - h_i)]}{\pi l(p_i - h_i)}$	0.5643
Spherical mask (diameter $d = 0.6667$)	0.6248	$3\left(\frac{\sin[\pi d\lvert\mathbf{p}-\mathbf{h}\rvert]}{[\pi d\lvert\mathbf{p}-\mathbf{h}\rvert]^3} - \frac{\cos[\pi d\lvert\mathbf{p}-\mathbf{h}\rvert]}{[\pi d\lvert\mathbf{p}-\mathbf{h}\rvert]^2}\right)$	0.6248

The Fourier Transforms of the masks are given in the third column, and predicted FNC values are given in the fourth column. $\delta_{\mathbf{hp}}$ is the 3D Kronecker delta. The values for l and d are given in fractions of the width of the cube containing the mask. There is excellent agreement between the average FNC values and the predicted values.

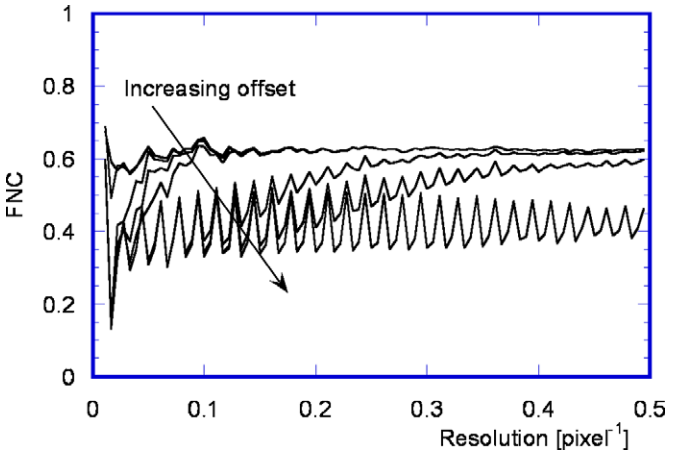

Fig. 3. Plot of the FNC for noise-filled spherical masks with different offsets in the noise. The arrow points in the direction of increasing offsets. The offsets in multiples of the standard deviation of the noise are 0, 1/200, 1/20, 1/10, 1/2, 2, and 5. A solid mask was used for the final plot giving the lowest FNC.

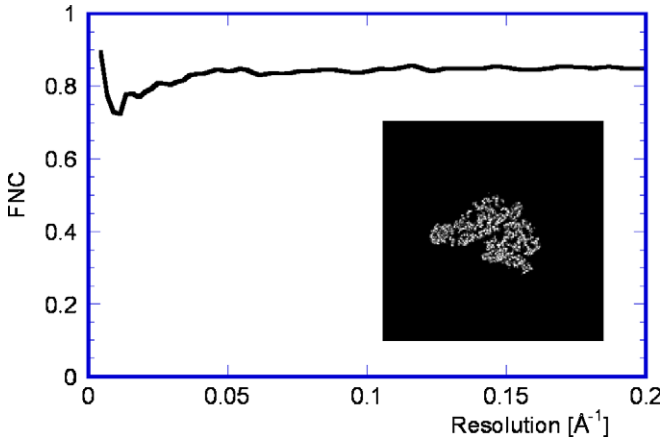

Fig. 4. Plot of the FNC for a density map generated from the atomic model of the 50S large ribosomal subunit (Klein et al., 2001, PDB code 1JJ2). The correlation between neighboring Fourier shells is more or less constant (about 0.85) across the spectrum. The inset shows a slice through the structure.

Unlike in the previous case, the FT of a solid cube of constant value is zero everywhere except at the origin where it assumes a value equal to the volume of the cube multiplied by the constant. When masking a cube filled with noise, correlation was introduced between Fourier terms that were random and uncorrelated. The correlation between Fourier terms in the transform of a solid cube is undefined since the terms are all zero (except at the origin). Therefore, arguments made for the behavior of the FNC do not apply in this case. The FNC of a solid mask depends on its FT, $G_{\mathbf{hp}}$, evaluated at points $\mathbf{p}$ while keeping $\mathbf{h} = 0$, i.e., at point where $|\mathbf{p} - \mathbf{h}| \geqslant 1$.

Coming back to the plots shown in Fig. 3, it can now be seen that the FNC in each plot has two regimes. At low resolution it is determined by the FT of the solid mask, while at high resolution it follows the behavior described earlier and remains approximately constant. The extent of each regime depends on the value of the offset. The discussion of offsets brings us closer to the expected FNC calculated for a real macromolecular structure. To a first approximation, such a structure can also be thought of as having a low-resolution component that produces a constant offset in the density distribution, while the finer details of the structure can be modeled as having randomly distributed density values. Clearly, this approximation represents an oversimplification of a real structure. The density of a real structure will, in general, be variable at low resolution due to the presence of domains that appear as regions of higher density, separated by regions of lower density. Any flexible or disordered regions within the structure will also lead to attenuated density, compared with other regions that are more ordered (see below). Finally, the density of protein and nucleic acid differs, leading to density variations in complexes containing both proteins and nucleic acids (Spahn et al., 2000). At higher resolution, the density is not randomly distributed due to secondary structure, such as α-helices and β-sheets. Furthermore, periodic features in the structure may give rise to strong Fourier terms at higher resolution, producing deviations from a constant FNC. Keeping these potential problems in mind, we look at the FNC of a 3D density map generated from the atomic model of the 50S large ribosomal subunit (Klein et al., 2001), PDB code 1JJ2 using SPIDER (Frank et al., 1996). This model contains both proteins and nucleic acids and is, therefore, a good test case for our purpose. The density was rendered with a pixel size of 2.44 Å, roughly centered in a box with 180 pixels along each side. The mask transform $G_{\mathbf{hp}}$ (Eq. 2) now describes the envelope of the structure. Fig. 4 shows the FNC plot for this structure calculated using Eq. (3). The correlation between terms in neighboring Fourier shells is more or less constant across the spectrum (in this case FNC ≈ 0.85). There is significant deviation from this value only at very low resolution, suggesting that the behavior of the FNC is similar to the behavior found for the noise-filled spherical mask (see Fig. 3). This encouraged us to develop the theory further to allow the measurement of the signal-to-noise ratio (SNR) of a structure that contains an additional noise term.

2.3. Measuring the signal-to-noise ratio

For a structure containing an additional noise term we assume that we have density arising from a macromolecular structure, such as the 50S large ribosomal subunit (see Fig. 4). This will be referred to as the signal. The additional noise is assumed to be background with Gaussian-distributed density that is entirely uncorrelated with the structure. This assumption appears to be reasonable for real structures determined by electron microscopy (Penczek et al., 2006). We define FNC_F as the constant describing the FNC arising from the structure in the high-resolution regime, where we expect an approximately constant FNC

(see Fig. 4). The background (noise) may fill the entire cube containing the structure, or it may fill only part of it. For example, the background might be present only inside a sphere containing the structure, and density values outside the sphere are set to a constant, i.e., they do not contribute to the variance of the background. This situation corresponds to most 3D reconstructions calculated from single particle images, as densities outside a spherical mask are usually set to a constant equal to the average density of the background. We will refer to this mask as the background mask. In the following we also assume that the variance of the noise is, on average, the same everywhere inside the background mask, or throughout the cube if no background mask was applied. This assumption may not be true for reconstructions of real structures, as will be discussed below. We define FNC_N as the constant describing the FNC arising solely from the background. If the background fills the entire cube containing the structure, $FNC_N = 0$ (see Fig. 2). If the background does not fill the entire cube $FNC_N > 0$ (see Fig. 2).

We rewrite Eq. (3) by replacing the Fourier terms $F_{\mathbf{p}}$ and $F_{\mathbf{h}}$ by $F_{\mathbf{p}} + N_{\mathbf{p}}$ and $F_{\mathbf{h}} + N_{\mathbf{h}}$, respectively, to indicate the additional noise term. The FNC is then given by

$$\begin{aligned}\mathrm{FNC}(R) &= \frac{\sum_{\mathbf{p}\in R'<p\leqslant R}\sum_{\mathbf{h}\in N(\mathbf{p})}(F_{\mathbf{p}}+N_{\mathbf{p}})(F_{\mathbf{h}}+N_{\mathbf{h}})^*}{\sqrt{\sum_{\mathbf{p}\in R'<p\leqslant R}\sum_{\mathbf{h}\in N(\mathbf{p})}\left|(F_{\mathbf{p}}+N_{\mathbf{p}})\right|^2\sum_{\mathbf{p}\in R'<p\leqslant R}\sum_{\mathbf{h}\in N(\mathbf{p})}\left|(F_{\mathbf{h}}+N_{\mathbf{h}})\right|^2}} \\ &\approx \frac{\sum_{\mathbf{p}\in R'<p\leqslant R}\sum_{\mathbf{h}\in N(\mathbf{p})}(F_{\mathbf{p}}F_{\mathbf{h}}^*+N_{\mathbf{p}}N_{\mathbf{h}}^*)}{\sqrt{\sum_{\mathbf{p}\in R'<p\leqslant R}\sum_{\mathbf{h}\in N(\mathbf{p})}\left(|F_{\mathbf{p}}|^2+|N_{\mathbf{p}}|^2\right)\sum_{\mathbf{p}\in R'<p\leqslant R}\sum_{\mathbf{h}\in N(\mathbf{p})}(|F_{\mathbf{h}}|^2+|N_{\mathbf{h}}|^2)}} \\ &= \frac{FNC_F\sqrt{\mathrm{SNR}(R)\mathrm{SNR}'(R)+FNC_N}}{\sqrt{(\mathrm{SNR}(R)+1)(\mathrm{SNR}'(R)+1)}}. \end{aligned} \tag{4}$$

In the approximation in Eq. (4), it is assumed that the sums over cross terms between the signal and the background are small compared to other terms and can be ignored. The signal-to-noise ratios (variance ratio of signal and noise) $\mathrm{SNR}(R)$ and $\mathrm{SNR}'(R)$ are given by

$$\mathrm{SNR}(R) = \frac{\sum_{\mathbf{p}\in R'<p\leqslant R}\sum_{\mathbf{h}\in N(\mathbf{p})}|F_{\mathbf{p}}|^2}{\sum_{\mathbf{p}\in R'<p\leqslant R}\sum_{\mathbf{h}\in N(\mathbf{p})}|N_{\mathbf{p}}|^2} \tag{5}$$

and

$$\mathrm{SNR}'(R) = \frac{\sum_{\mathbf{p}\in R'<p\leqslant R}\sum_{\mathbf{h}\in N(\mathbf{p})}|F_{\mathbf{h}}|^2}{\sum_{\mathbf{p}\in R'<p\leqslant R}\sum_{\mathbf{h}\in N(\mathbf{p})}|N_{\mathbf{h}}|^2}. \tag{6}$$

We assume that the SNR does not change significantly from resolution shell to resolution shell and, therefore, $\mathrm{SNR}(R) \approx \mathrm{SNR}'(R)$. It follows that

$$\mathrm{FNC}(R) \approx \frac{FNC_F\mathrm{SNR}(R) + FNC_N}{(\mathrm{SNR}(R)+1)} \tag{7}$$

and

$$\mathrm{SNR}(R) = \frac{FNC_N - \mathrm{FNC}(R)}{\mathrm{FNC}(R) - FNC_F}. \tag{8}$$

Eq. (8) provides a way to calculate the SNR of a structure given the average FNC in a resolution shell R between neighboring terms in the FT of the structure, the expected correlation coefficients for the noise-free structure, FNC_F, and the noise alone, FNC_N. FNC_F and FNC_N can be estimated using a masking procedure (see below). It is important to remember that Eqs. (4), (7) and (8) are only valid in the regime, where the FNC of the signal is approximately constant. At very low resolution, the FNC depends strongly on the details of the FT of the molecular envelope, $G_{\mathbf{hp}}$, with $|\mathbf{p}-\mathbf{h}| > 1$ and the SNR cannot be calculated using Eq. (8). The SNR in Eq. (8) can be related to the FSC that is commonly determined between two structures that are each calculated from one half of the data set to measure the resolution of the combined structure (Grigorieff, 2000):

$$\mathrm{SNR}(R) = \frac{2\mathrm{FSC}(R)}{1-\mathrm{FSC}(R)}. \tag{9}$$

Therefore,

$$\mathrm{FSC}(R) = \frac{\mathrm{FNC}(R) - FNC_N}{2FNC_F - FNC_N - \mathrm{FNC}(R)}. \tag{10}$$

To test the predicted correspondence between the FNC and FSC given in Eq. (10), the density map generated from the atomic model of the 50S large ribosomal subunit (see Fig. 4) was low-pass filtered using a Gaussian (filter radius 1/8.13 Å^{-1}). This map was used to generate two new maps, each with added Gaussian-distributed noise at a SNR of 1/5. In this simulation, these two maps represent the two reconstructions usually calculated from the two halves of an experimentally obtained data set. The FSC between these two maps is plotted in Fig. 5B. The two maps were then added to generate a new map with an SNR of 2/5. This represents the final reconstruction calculated from the entire experimentally obtained data set. The predicted FSC (Eq. 10) was calculated for the summed map and is also plotted in Fig. 5B. To estimate the constants, FNC_F and FNC_N, the masking procedure described in the next section was used. The measured and predicted FSC curves match almost perfectly, except at low resolution (see above). Therefore, these simulations validate the approach described in this section.

2.4. Structural flexibility and disorder

As mentioned above, one reason for variation of density within a structure may be flexibility or disorder of parts of the structure. To investigate effects of disorder on the FNC and predicted FSC, the map derived from the atomic model of the 50S large ribosomal subunit was used (see Fig. 5A). Disorder on the periphery of the structure was simulated by producing a low-pass filtered structure using a box convolution (operation BC in the image processing package SPIDER, Frank et al., 1996). The size of the convolution box was about $15\times15\times15$ Å ($6\times6\times6$ pixels). The densities in the center of this low-pass filtered map were set to zero using a spherical mask with a diameter of about 146 Å (60 pixels) and a cosine edge of 15 Å width (6 pixels, operation MA in the image processing package

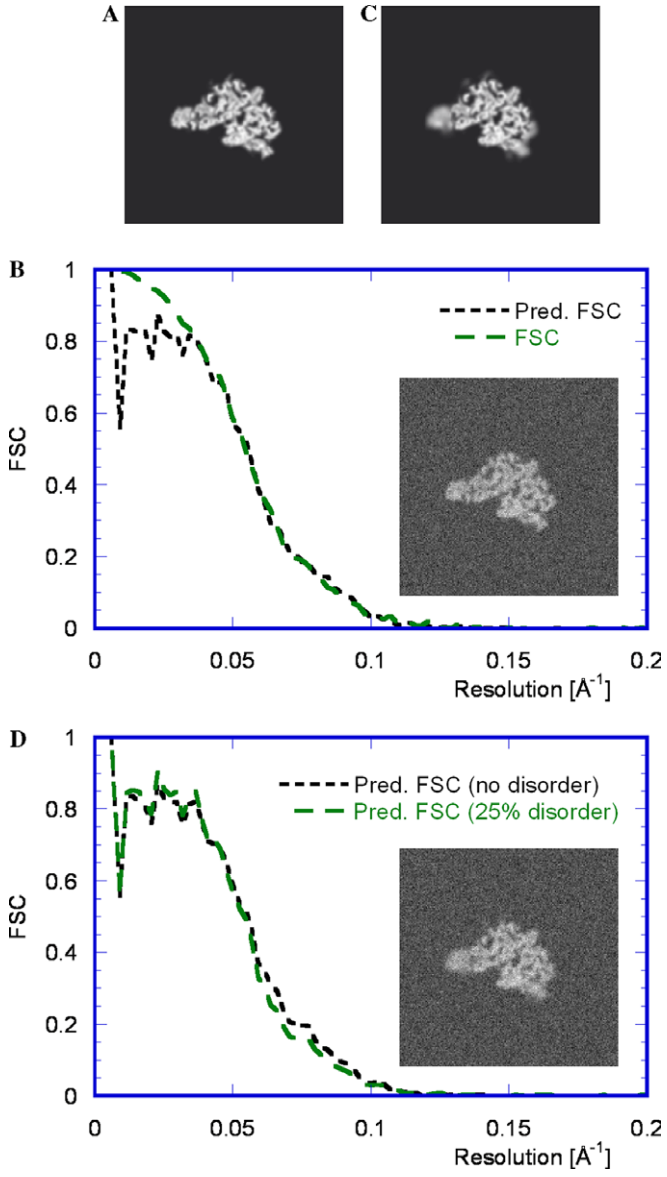

Fig. 5. Noise and disorder in a structure. (A) shows a slice through a low-pass filtered version of the 50S density map shown in Fig. 4. (B) Fourier Shell Correlation (FSC) between two noisy representations (SNR = 1/5) of the density map in (A), and FNC-based Fourier Shell Correlation (Pred. FSC) evaluated for the sum of the two density maps (SNR = 2/5). The inset shows a slice through the latter map. (C) shows a slice through a low-pass filtered version of the 50S density map shown in Fig. 4, with additional low-pass filtering of peripheral domains to simulate disorder (25% of the total volume of the structure). (D) Same FNC-based Fourier Shell Correlation as in (B), and FNC-based Fourier Shell Correlation of map shown in (C) with noise (SNR = 2/5). A drop in the latter FSC is visible at about 15 Å resolution and above.

SPIDER). The opposite mask was applied to the unfiltered map to select the density inside a sphere with a diameter of about 146 Å. The two masked maps were then added together, resulting in a map with more defined density in the center and smeared-out density on the periphery (Fig. 5C). The volume of the smeared-out density corresponded to about 25% of the volume of the 50S density. The predicted FSC (Fig. 5D) is essentially unchanged compared with the structure prior to box convolution. The main difference occurs at about 15 Å resolution and above were a slight drop in the FSC can be observed for the smeared-out structure, consistent with the signal loss at that resolution. However, there is also a small difference visible between the two FSC curved below about 30 Å resolution, indicating that density variations within the structure have a small effect on the FNC and predicted FSC at low resolution.

2.5. Over-fitting of noise

As a final simulated test, the new algorithm was used with a structure that was reconstructed from 30 000 projections of the 50S map, filtered using a Gaussian low-pass filter with a radius of 1/24.4 Å^{-1}. This test was similar to tests run previously to investigate over-fitting during refinement (Stewart and Grigorieff, 2004). The pixel size was increased to 4.88 Å to speed up the calculation. A CTF was applied to produce images similar to those obtained from an electron microscope. The CTF did not have an envelope attenuating its amplitude towards high resolution. Defocus values for the CTF varied between 40 and 60 in generalized units (Wade, 1992). Finally, Gaussian noise was added to the projection images to give an SNR of 1/100. The parameters describing the orientations and positions of each particle in this data set were perturbed by addition of random, uniformly distributed angles with a standard deviation of about 10° and random, uniformly distributed displacements with a standard deviation of about two pixels. Nine cycles of refinement were carried out using the program FREALIGN (Grigorieff, 2006) and employing a linear correlation coefficient for the alignment between

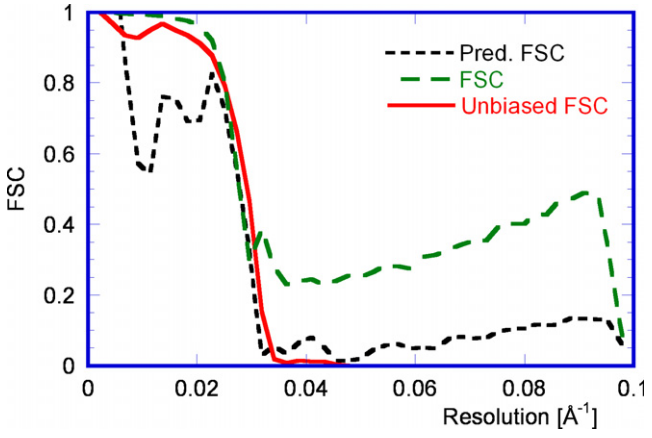

Fig. 6. Over-fitting of noise during refinement. The FNC-based Fourier Shell Correlation (Pred. FSC) and traditional Fourier Shell Correlation (FSC) for the 50S large ribosomal subunit after refinement and reconstruction from 30 000 computer-generated noisy projections (SNR = 1/100) are shown. For comparison, the unbiased FSC (Unbiased FSC) was obtained by comparison of the refined structure with the original noise-free density map generated from the atomic model of the 50S large ribosomal subunit (see text). The unbiased FSC shows that the traditional FSC determined from two halves of the data set suffers from noise bias. The FNC-based FSC follows more closely the unbiased FSC.

the images and the reference. FREALIGN normally uses a weighted correlation coefficient for the alignment to reduce over-fitting of noise (Stewart and Grigorieff, 2004). Fig. 6 shows the resulting FSC curves after refinement. The FSC curve comparing two reconstructions calculated by dividing the data set in two halves (labeled FSC in Fig. 6) is close to 1 at low resolution, drops to about 0.25 in the intermediate resolution range, and then increases again to about 0.5 at higher resolution. This behavior is characteristic for a reconstruction that suffers from over-fitting of noise (Stewart and Grigorieff, 2004). When comparing the final reconstruction with the noise-free structure used to generate the projections, a second FSC curve can be calculated and converted to a curve that is equivalent to the FSC measured between the reconstructions calculated from two halves of the data (Rosenthal and Henderson, 2003). This curve is also shown in Fig. 6 (labeled Unbiased FSC) and clearly shows that the resolution of the refined structure is significantly lower than indicated by the first curve. Finally, the FSC curve calculated from the FNC is plotted (Predicted FSC). Although it does not entirely agree with the unbiased FSC, it is very close and indicates the correct resolution much more reliably than the traditional FSC curve. This is an important result because it suggests that the new algorithm can be used as a more unbiased resolution measurement for the general evaluation of single particle reconstructions.

2.6. Masking procedure

The values for FNC_F and FNC_N can be estimated from noise-filled masks describing the structure and background, respectively, by calculating the average FNC across the entire spectrum (see above and Table 1). For the determination of a tight mask for the structure we developed a procedure that is based on the density histogram of a low-pass filtered version of the structure. We will refer to this mask as the structure mask. As a low-pass filter we chose a Gaussian-shaped filter with a radius of 1/20 $Å^{-1}$ to retain sufficient information about the shape of the structure, but without finer and noisier detail. This helps in determining the correct threshold for the structure mask. A typical histogram of densities sorted into 100 bins is shown in Fig. 7A, calculated from a filtered reconstruction of the *Escherichia coli* 70S ribosome (Gabashvili et al., 2000, EMD code 1003). There are three distinct regions. At the low density end is a large peak that contains pixels in the reconstruction that are part of the background. The histogram has a plateau in the middle region where contributing densities are above the background, but still clearly below the density peaks of the structure that represent the strongest features. An appropriate density threshold to define a binary mask for the structure will lie in this plateau region. The third region represents the strongest density features and sometimes shows a second peak, as in Fig. 7A, but can also simply be the beginning of a steady decline towards zero.

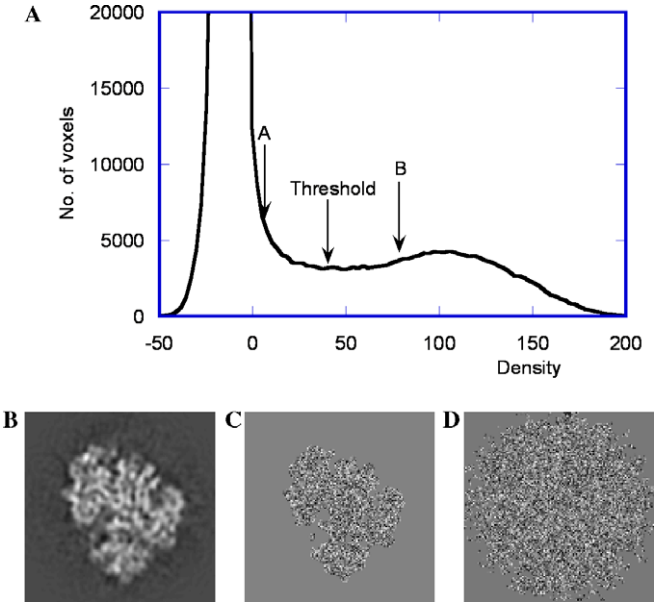

Fig. 7. (A) Density histogram of a low-pass filtered version of the *E. coli* 70S ribosome, solved by single particle electron microscopy (Gabashvili et al., 2000, EMD code 1003). Slices through the untreated 70S density map (B), the corresponding structure mask (C) and background mask (D) are shown.

In a first step, approximate boundaries of the middle plateau region are established. The second derivative of the histogram helps in this process. To reduce random fluctuations in the second derivative, a running average over seven histogram bins is calculated. Starting from the maximum in the histogram and approaching higher densities, the second derivative will have a maximum where the large peak (the first region) transitions into the plateau region. This maximum will be taken as the left boundary of the plateau region. The right boundary of the plateau region is characterized by a negative second derivative that indicates either an accelerated decline of the histogram towards zero, or the approach of the second peak in the histogram, as in Fig. 7A. To avoid picking an accidental negative second derivative that may occur at an isolated point within the plateau region, we require that five points within a contiguous interval of six points on the second derivative are negative. Although this is a somewhat arbitrary criterion, it identifies the right boundary of the plateau region very reliably when testing the algorithm on a number of structures from the EM database. The density threshold for generating a binary mask from the low-pass filtered structure is then picked as the mid point between the two boundaries of the plateau region. Fig. 7C shows the outline of the structure mask determined for the *E. coli* 70S ribosome as an example.

For the value of FNC_N, the part of the cube containing background has to be determined. This is done by calculating the local variance at each point outside the structure mask. The local variance is calculated by including the pixel value at a point and the values of all surrounding pixels (a total of 27 pixels). If a prior mask (the background

mask, see above) was applied to the reconstruction, the local variance will vanish outside this mask. The background mask for the noise is then determined by including all pixels with a local variance above a certain threshold. In practice, it was found that a threshold of half the average variance (not including the volume containing the structure) led to a good representation of the part of the volume containing background. The background mask, however, will also include the volume inside the structure mask since it is assumed that the noise level of the background is the same within and outside the structure (see above). The background mask is then filled with random density values, similar to the procedure for FNC_F. FNC_N is calculated as the average FNC in the FT of this mask. Fig. 7D shows the outline of the background mask determined for the *E. coli* 70S ribosome as an example.

3. Application to experimental data

The algorithms described above were implemented in a program called RMEASURE. Its only inputs are the density map of the structure and the pixel size in Å. The outputs are FNC and predicted FSC curves. The program was tested on two experimental cases, the *E. coli* 70S ribosome (Gabashvili et al., 2000, EMD code 1003), and a recently determined structure of the ryanodine receptor (Samso et al., 2005). Fig. 8A shows the result for the ribosome structure. The published FSC curve drops below 0.5 at 11.5 Å (Gabashvili et al., 2000), and below 0.143 at about 9.6 Å resolution. The FSC curve predicted by RMEASURE drops below 0.5 at 12.5 Å, and below 0.143 at 10.4 Å resolution. The predicted curve is, therefore, close to the published FSC curve at a resolution above 30 Å, and a resolution measurement based on the predicted curve would be compatible with the resolution estimate obtained from the traditional FSC curve. At a resolution below 30 Å, the predicted FSC curve drops well below the published curve. A drop at low resolution is also observed with the simulated data in the previous section and indicates the low-resolution regime where the FNC depends on details of the molecular transform. However, this has no effect on the predicted resolution limits based on the 0.5 and 0.143 thresholds.

Fig. 8B shows the results for the ryanodine receptor (Samso et al., 2005). The predicted FSC curve shows even closer agreement with the traditional FSC curve measured between two reconstructions from two halves of the data. Both curves drop below a value of 0.5 at about 13 Å resolution, and below 0.143 at about 10 Å resolution. The predicted FSC curve again shows a significant drop below 50 Å resolution.

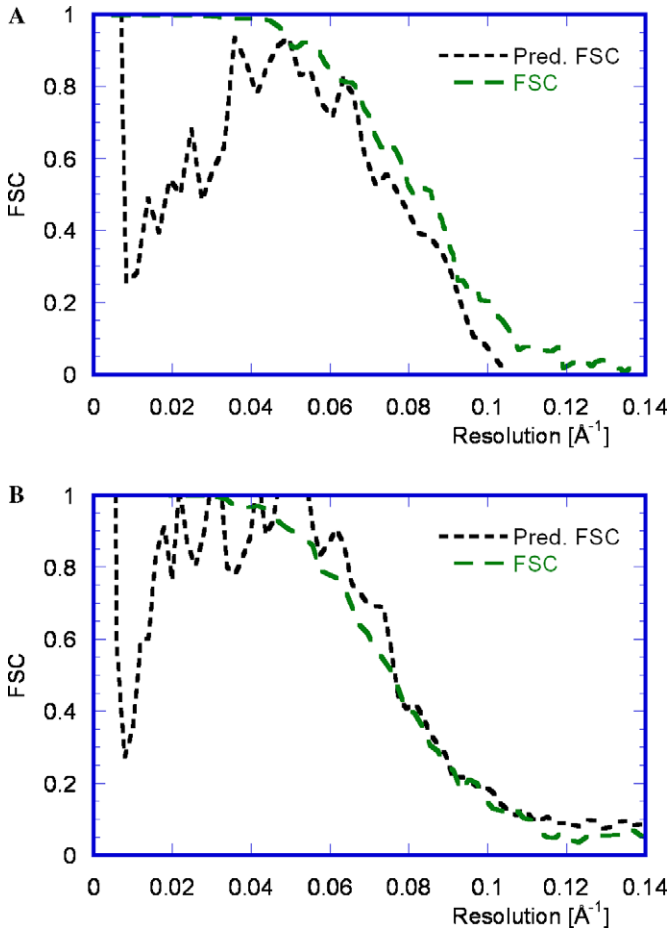

Fig. 8. FNC-based Fourier Shell Correlation (Pred. FSC) and traditional Fourier Shell Correlation (FSC) for two experimentally obtained reconstructions. (A) *E. coli* 70S ribosome (Gabashvili et al., 2000, EMD code 1003), and (B) ryanodine receptor (Samso et al., 2005).

4. Discussion

The new method described here for assessing the resolution of a reconstruction does not require the original data used to calculate the reconstruction. It is, therefore, easier to use and more widely applicable than the more traditional methods. The simulations shown in Figs. 5 and 6 demonstrate that the FNC and the theoretical considerations described here provide an accurate method to measure the SNR of a 3D reconstruction as a function of resolution. Furthermore, according to the simulation shown in Fig. 6, this measurement seems to be less affected by over-fitting of noise in a refined structure compared with the traditional FSC.

The dependence of the FNC on over-fitting of noise resulting from refinement of a structure deserves further discussion. The bias in the FSC measuring the correlation between two reconstructions calculated from two halves of the data was recently discussed (Grigorieff, 2000; Shaikh et al., 2003; Stewart and Grigorieff, 2004). It arises essentially from the partial alignment of the noise in the images to the reference used in the refinement. The aligned noise leads to additional artificial correlation between the two reconstructions calculated from two halves of the data. Structures that suffer from over-fitting of noise usually display high-resolution detail that does not correspond with actual structural features of the sample. In other words, the refinement procedure "invents" these details. In the

assessment of the structure, it is often not possible to distinguish true structural detail from artifact. Shaikh et al. proposed a cross-validation method in which part of the image data is excluded from the alignment and refinement. This approach is, therefore, akin to the free R-factor used in X-ray crystallography. To make their assessment compatible with other resolution measures, data in entire resolution zones are excluded. Any correlation observed in these resolution zones between reconstructions from two halves of the data should then be unbiased. As noted by the authors, it is important that the resolution zones containing the excluded data encompass sufficiently large intervals in Fourier space to avoid bias from neighboring Fourier terms corresponding to data that was included in the refinement. The potential bias is due to the same correlation between Fourier terms that is used here to measure the SNR of a reconstruction. The FNC is not based on cross-validation and it is, therefore, not so obvious why it is less sensitive to over-fitting. Indeed, the FNC for the signal, FNC_F, is calculated from a mask filled with random noise, completely uncorrelated with high-resolution detail of the reconstruction, whether true or not. In the method described here, the distinction between signal and noise is made by the masking procedure (see above). Any density inside the structure mask counts as signal plus noise, whereas any density outside this mask counts as noise. For the measurement of the SNR, the noise level within the mask is assumed to be the same as elsewhere in the volume (see Section 2 above). If this condition is not met, the calculation of the SNR will be inaccurate. For example, if the noise level within the structure mask is higher than elsewhere, part of the variance of this noise will be counted as signal, and the measured SNR will be higher than the true SNR. If over-fitting of noise occurs in the refinement of a structure, noise in the images within and outside the area of the particle will be aligned to the reference. This will give rise to additional features and density variance within and outside the structure (Grigorieff, 2000; Stewart and Grigorieff, 2004). As long as the variance increase per pixel is the same everywhere, it will not influence the measurement of the SNR. This is the main reason for the FNC-based resolution measurement to be less affected by over-fitting of noise. However, in a reference, the density variance within the structure is usually much higher than outside the structure. Therefore, during the alignment of images to the reference, any features in the images that overlap with the density of the projected structure will receive a higher weight compared with other features. Therefore, the noise within the area of the particles receives a stronger bias to agree with the reference than noise elsewhere in the images (Stewart and Grigorieff, 2004). This leads to a higher noise level within the structure than outside it. Therefore, a small bias in the measurement of the SNR remains, and is indeed visible in Fig. 6. The use of an appropriate weighting scheme for the data during alignment can minimize this effect. Such a weighting scheme was implemented, for example, in the program FREALIGN (Stewart and Grigorieff, 2004).

The method described here breaks down at low resolution where the FNC depends on details of the molecular transform of the structure. Deviations between the FNC-based FSC and the FSC calculated between reconstructions each containing half the data can be substantial at low resolution (Fig. 8A). However, this does not normally influence the resolution assessment of the structure which is determined by the SNR and FSC at higher resolution. The FNC at low resolution can be influenced by several factors, such as density variations due to flexibility or disorder in the structure that produce non-uniform resolution (see Fig. 5C). Problems may also occur if the resolution is non-isotropic, i.e., it varies with direction within the structure. Such a variation may, for example, be caused by preferred views of the particle during data collection, or if the structure contains strong periodic features. Resolution estimation may also be hindered by tight masking of the structure resulting in the masks for the structure and the background to be essentially the same. This leads to similar values for FNC_F and FNC_N in Eq. (10) which can then not be used for calculating the FSC. However, in cases where masking is not a problem, as with the structures determined for the *E. coli* 70S ribosome and the ryanodine receptor (see Fig. 8), a reasonable FNC-based resolution estimate can be obtained.

It is worth adding a comment here about the deposition of 3D structures in the EM Database (http://www.ebi.ac.uk/msd-srv/emsearch/). The deposition of published structures determined by electron microscopy is strongly encouraged and a growing number of structures have already been deposited. For the deposited data to be useful, however, it is important that structures are deposited without extensive "editing", such as tight masking or filtering with a sharp resolution cut-off. Tight masking or filtering removes valuable information about a structure, such as levels of noise and background. It also often introduces artifacts, such as sharp edges where tight masks cut into the density of the structure, or ripples where sharp filters are used. The deposition of a structure "as is", unmasked and unfiltered, and possibly a second structure masked and filtered to the appropriate resolution should become the standard.

Acknowledgments

Inspiring discussions with Pawel Penczek are gratefully acknowledged. The authors are grateful to Montserrat Samsó for making the reconstruction of the ryanodine receptor available. N.G. gratefully acknowledges financial support by the National Institutes of Health, Grant 1 P01 GM-62580, and by a research fellowship from the Humboldt Foundation. The authors were also supported by Grant 1 R01 GM-63012.

References

Arnold, E., Rossmann, M.G., 1986. Effect of errors, redundancy, and solvent content in the molecular replacement procedure for the

structure determination of biological macromolecules. Proc. Natl. Acad. Sci. USA 83, 5489–5493.

Bottcher, B., Wynne, S.A., Crowther, R.A., 1997. Determination of the fold of the core protein of hepatitis B virus by electron cryomicroscopy. Nature 386, 88–91.

Frank, J., Radermacher, M., Penczek, P., Zhu, J., Li, Y., Ladjadj, M., Leith, A., 1996. SPIDER and WEB: processing and visualization of images in 3D electron microscopy and related fields. J. Struct. Biol. 116, 190–199.

Frank, J., Verschoor, A., Boublik, M., 1981. Computer averaging of electron micrographs of 40S ribosomal subunits. Science 214, 1353–1355.

Gabashvili, I.S., Agrawal, R.K., Spahn, C.M., Grassucci, R.A., Svergun, D.I., Frank, J., Penczek, P., 2000. Solution structure of the *E. coli* 70S ribosome at 11.5A resolution. Cell 100, 537–549.

Grigorieff, N., 2000. Resolution measurement in structures derived from single particles. Acta Crystallogr. D Biol. Crystallogr. 56 (Pt 10), 1270–1277.

Grigorieff, N., 2006. FREALIGN: high-resolution refinement of single particle structures. J. Struct. Biol..

Halic, M., Gartmann, M., Schlenker, O., Mielke, T., Pool, M.R., Sinning, I., Beckmann, R., 2006. Signal recognition particle receptor exposes the ribosomal translocon binding site. Science 312, 745–747.

Harauz, G., van Heel, M., 1986. Exact filters for general geometry 3-dimensional reconstruction. Optik 73, 146–156.

Henderson, R., 1995. The potential and limitations of neutrons, electrons and X-rays for atomic resolution microscopy of unstained biological molecules. Q. Rev. Biophys. 28, 171–193.

Jurica, M.S., Sousa, D., Moore, M.J., Grigorieff, N., 2004. Three-dimensional structure of C complex spliceosomes by electron microscopy. Nat. Struct. Mol. Biol. 11, 265–269.

Klein, D.J., Schmeing, T.M., Moore, P.B., Steitz, T.A., 2001. The kink-turn: a new RNA secondary structure motif. EMBO J. 20, 4214–4221.

Laurinmaki, P.A., Huiskonen, J.T., Bamford, D.H., Butcher, S.J., 2005. Membrane proteins modulate the bilayer curvature in the bacterial virus Bam35. Structure 13, 1819–1828.

Ludtke, S.J., Chen, D.H., Song, J.L., Chuang, D.T., Chiu, W., 2004. Seeing GroEL at 6 A resolution by single particle electron cryomicroscopy. Structure 12, 1129–1136.

Nogales, E., Grigorieff, N., 2001. Molecular machines: putting the pieces together. J. Cell Biol. 152, F1–F10.

Penczek, P.A., Grassucci, R.A., Frank, J., 1994. The ribosome at improved resolution: new techniques for merging and orientation refinement in 3D cryo-electron microscopy of biological particles. Ultramicroscopy 53, 251–270.

Penczek, P.A., Yang, C., Frank, J., Spahn, C.M., 2006. Estimation of variance in single-particle reconstruction using the bootstrap technique. J. Struct. Biol. 154, 168–183.

Rosenthal, P.B., Henderson, R., 2003. Optimal determination of particle orientation, absolute hand, and contrast loss in single-particle electron cryomicroscopy. J. Mol. Biol. 333, 721–745.

Samso, M., Wagenknecht, T., Allen, P.D., 2005. Internal structure and visualization of transmembrane domains of the RyR1 calcium release channel by cryo-EM. Nat. Struct. Mol. Biol. 12, 539–544.

Shaikh, T.R., Hegerl, R., Frank, J., 2003. An approach to examining model dependence in EM reconstructions using cross-validation. J. Struct. Biol. 142, 301–310.

Sokolova, O., Kolmakova-Partensky, L., Grigorieff, N., 2001. Three-dimensional structure of a voltage-gated potassium channel at 2.5 nm resolution. Structure (Camb) 9, 215–220.

Spahn, C.M., Penczek, P.A., Leith, A., Frank, J., 2000. A method for differentiating proteins from nucleic acids in intermediate-resolution density maps: cryo-electron microscopy defines the quaternary structure of the *Escherichia coli* 70S ribosome. Structure 8, 937–948.

Stewart, A., Grigorieff, N., 2004. Noise bias in the refinement of structures derived from single particles. Ultramicroscopy 102, 67–84.

Unser, M., Trus, B.L., Frank, J., Steven, A.C., 1989. The spectral signal-to-noise ratio resolution criterion: computational efficiency and statistical precision. Ultramicroscopy 30, 429–433.

Unser, M., Trus, B.L., Steven, A.C., 1987. A new resolution criterion based on spectral signal-to-noise ratios. Ultramicroscopy 23, 39–51.

Wade, R.H., 1992. A brief look at imaging and contrast transfer. Ultramicroscopy 46, 145–156.

Zhang, X., Walker, S.B., Chipman, P.R., Nibert, M.L., Baker, T.S., 2003. Reovirus polymerase lambda 3 localized by cryo-electron microscopy of virions at a resolution of 7.6 A. Nat. Struct. Biol. 10, 1011–1018.

Zhou, Z.H., Baker, M.L., Jiang, W., Dougherty, M., Jakana, J., Dong, G., Lu, G., Chiu, W., 2001. Electron cryomicroscopy and bioinformatics suggest protein fold models for rice dwarf virus. Nat. Struct. Biol. 8, 868–873.